Indium-Gallium Segregation in $CuIn_xGa_{1-x}Se_2$: An *Ab Initio*–Based Monte Carlo Study

Christian D. R. Ludwig, Thomas Gruhn, and Claudia Felser
Institute of Inorganic and Analytical Chemistry, Johannes Gutenberg-Universität Mainz, Germany

Tanja Schilling
Institute of Physics, Johannes Gutenberg-Universität Mainz, Germany
Theory of Soft Condensed Matter, Université du Luxembourg, Luxembourg

Johannes Windeln
IBM Mainz, Germany

Peter Kratzer
Faculty of Physics, Universität Duisburg-Essen, Germany
(Received 7 April 2010; revised manuscript received 11 June 2010; published 9 July 2010)

Thin-film solar cells with $CuIn_xGa_{1-x}Se_2$ (CIGS) absorber are still far below their efficiency limit, although lab cells already reach 20.1%. One important aspect is the homogeneity of the alloy. Large-scale simulations combining Monte Carlo and density functional calculations show that two phases coexist in thermal equilibrium below room temperature. Only at higher temperatures, CIGS becomes more and more a homogeneous alloy. A larger degree of inhomogeneity for Ga-rich CIGS persists over a wide temperature range, which contributes to the observed low efficiency of Ga-rich CIGS solar cells.

DOI: 10.1103/PhysRevLett.105.025702 PACS numbers: 64.75.Qr, 61.43.Bn, 84.60.Jt, 88.40.jn

As resources of fossil fuels are dwindling, alternative sources of energy gain increasing importance. The contribution of solar cells is continuously growing, and a lot of effort has been made to improve the efficiency. During the past years chalcopyrites like $CuIn_xGa_{1-x}Se_2$ (CIGS) have been shown to be promising absorber materials for thin-film solar cells with high efficiency and low production cost. Previous investigations have dealt with grain boundaries [1,2], defects [3], doping [4], film morphology in epitaxial growth [5], and inhomogeneities [6]. All these issues have an impact on the CIGS cell performance.

In this paper, we focus on the influence of the In-Ga ratio on the cell efficiency, which is not yet well understood. Pure $CuInSe_2$ has a band gap of 1.0 eV and $CuGaSe_2$ of 1.7 eV. Aiming at an optimal band gap for the absorption of the solar spectrum, an alloy with about 70% Ga should yield the highest efficiency [7,8]. Experimentally, however, the best efficiencies have been reached with a much lower Ga content of only 30% [9]. To shed more light on this issue, we study the inhomogeneity of the In-Ga distribution by Monte Carlo (MC) simulations.

Knowledge on the impact of granularity on solar cell performance is still fragmentary, but inhomogeneities lead to band-gap fluctuations, which most certainly have a detrimental effect on the cell efficiency [6,10]. Several groups investigate experimentally the inhomogeneities in the In-Ga distribution for a fixed In-Ga ratio [11,12] or for varying In-Ga ratios [6,13]. Photoluminescence measurements by Gütay and Bauer indicate that a higher Ga content leads to larger inhomogeneities [6]. Even small fluctuations in the composition unfavorably affect the electronic and optical properties [10]. This is an important factor that diminishes the efficiency of solar cells.

In this Letter, we present a computer simulation study of the spatial distribution of In and Ga in CIGS. To make the calculations feasible, we keep Cu and Se fixed at their respective lattice sites and neglect other defects. It is common to tackle properties of semiconductors computationally by using density functional theory for calculating their electronic structure. Up to now, density functional theory–based calculations of CIGS compounds have been carried out only for small numbers of atoms and for the pure compounds $CuInSe_2$ and $CuGaSe_2$ [14]. In this Letter, we discuss pattern formation on larger length scales at various temperatures.

By using the cluster expansion (CE) method [15], we extracted interaction energies from electronic structure calculations and used these energies as input for MC simulations of large samples with an exceedingly high number of possible atomic configurations.

The basic idea of the CE is to expand the formation energy ΔE_f of a configuration into energy contributions of "cluster figures" (single atoms, pairs, triples, etc.):

$$\Delta E_f = J_0 + \sum_i J_i s_i + \sum_{i<j} J_{ij} s_i s_j + \cdots. \qquad (1)$$

The indices i and j run over all lattice sites, and s_m is -1 for In and $+1$ for Ga on lattice site m. Every figure is associated with a coefficient J that gives the energy contribution of the specific figure. Detailed descriptions of the CE method can be found in Refs. [15,16]. The coefficients

of the expansion are fitted to *ab initio* energies from electronic structure calculations. Figures with a low value of J are neglected to simplify the expression.

We calculated formation energies of 32 $CuIn_xGa_{1-x}Se_2$ structures [space group $I\bar{4}2d$; cf. [14] and Fig. 1(a)] by using the *ab initio* electronic structure program ABINIT [17,18]. For the MC simulations, it is necessary to vary the distribution of In and Ga (active atoms). Cu and Se atoms do not partake in the cluster expansion. The structures include supercells containing up to 32 atoms. Trouiller-Martins-type pseudopotentials were used with the generalized gradient approximation of Perdew, Burke, and Ernzerhof [19]. The cutoff energy for the plane waves was set to 70 hartree, and a k-point grid of $3 \times 3 \times 3$ or bigger was used. The positions of all atoms were relaxed until the maximum force on atoms was less than 10^{-3} hartree/bohr, and all three lattice parameters were relaxed until the stress was less than 10^{-5} hartree/bohr^3.

The effective cluster interactions defining the CE were obtained by a least-squares fit to ABINIT formation energies. The CE with the lowest cross-validation score of 1.3 meV contains one point figure, eight pair figures, two triple figures, and two quadruple figures. The effects of constituent strain and volume deformation [20] were not taken into account, since we expect only a minor influence on mixed states with a fixed In:Ga ratio.

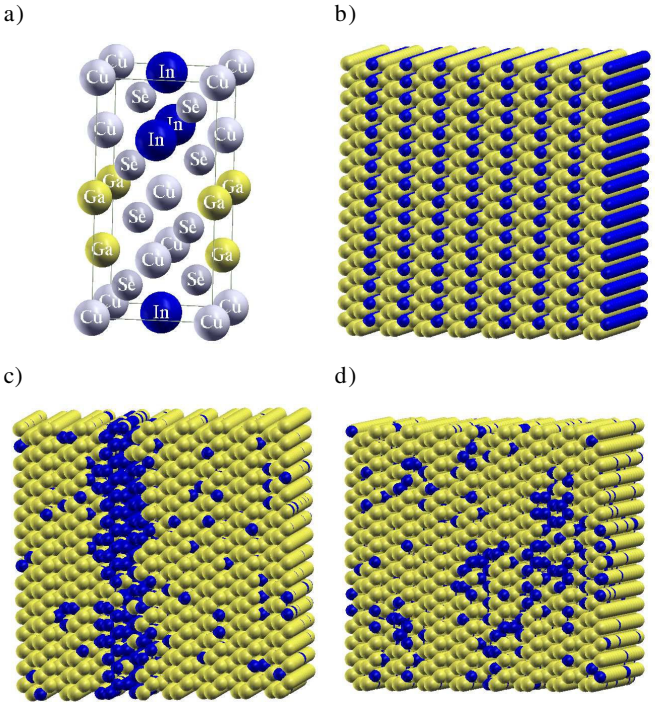

FIG. 1 (color online). (a) CIGS unit cells with In and Ga atoms on Wyckoff position 4b. (b) Snapshot of a system of periodic unit cells. (c) Snapshot of the Ga-rich system at 348 K. (d) Snapshot of the Ga-rich system at 406 K. Ga atoms are yellow; In atoms are blue. Cu and Se are not displayed in the snapshots, and the size of the spheres is arbitrary.

Canonical MC simulations were performed by using the CE to calculate configurational energies. One MC move consists of exchanging the position of two active atoms (In/Ga). The simulation box contained $16 \times 16 \times 8$ tetragonal CIGS unit cells (8192 active atoms). Simulations were run at temperatures between 290 (25 meV) and 870 K (75 meV, approximately the production temperature of CIGS solar cells) for 10^6 MC sweeps. Relaxation to the equilibrium state took less than 10^5 MC sweeps.

For data analysis the simulation box was divided into cubic segments of 16 lattice sites. The number of In (Ga) atoms b in each segment was counted and histograms were plotted. To have a measure for the inhomogeneity we computed the standard deviation σ of these distributions. (σ increases with increasing inhomogeneity.)

We have studied a system of $CuIn_{0.25}Ga_{0.75}Se_2$, which is in the following denoted as *Ga-rich* CIGS, and a system of $CuIn_{0.75}Ga_{0.25}Se_2$, which is denoted as *In-rich* CIGS.

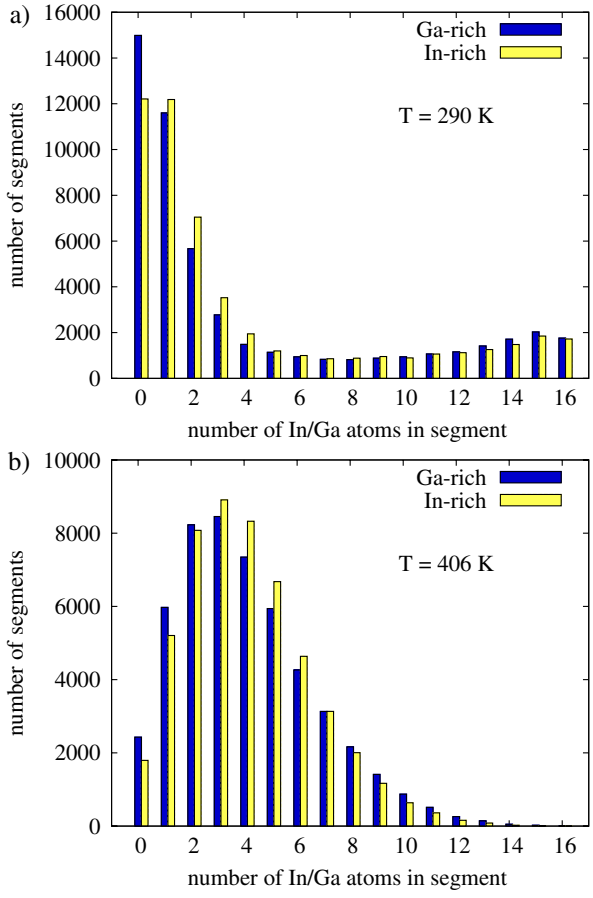

FIG. 2 (color online). Histograms showing the number of cubic segments in the simulation box that contain 1–16 atoms of a certain type. Blue is the distribution of In atoms in Ga-rich CIGS, and yellow is the distribution of Ga atoms in In-rich CIGS at temperatures of (a) 290 and (b) 406 K. A perfectly ordered In-rich or Ga-rich system would have 4 Ga/In atoms in every segment. The histogram would have all entries in bin 4.

Figure 2 shows histograms of the number of In (Ga) atoms in the segments for Ga-rich and In-rich CIGS. The temperature was kept constant at 290 and 406 K, respectively.

At 290 K the histograms have two maxima: one at the lower and one at the higher end of the scale. The majority of the segments contain very few or no In (Ga) atoms, but the small maximum indicates that a certain fraction of segments contain a large fraction of In (Ga) atoms. This means there are two phases: an In phase and a Ga phase. Both maxima are higher for Ga-rich CIGS. Close to the mean value of 4 the values for In-rich CIGS are higher. The standard deviation σ is 3.8% higher for Ga-rich CIGS, indicating a higher inhomogeneity (Table I).

At a temperature of 406 K the system has undergone a phase transition to a mixed, disordered phase. The histograms have changed drastically and show one broad peak with a long tail to the right. This is accompanied by a big change of σ to smaller values for both systems (Table I). The difference of the homogeneity is very pronounced; σ is 9.2% higher for Ga-rich CIGS, the largest difference for all considered temperatures (Table I). At higher temperatures the shape of both histograms becomes narrower and the difference between In-rich and Ga-rich CIGS becomes smaller (Table I).

Table I contains the σ values for more temperatures, for which no histograms are shown. It can be seen that σ is smaller for In-rich CIGS at all temperatures and σ decreases with temperature for both systems. The relative difference between In-rich and Ga-rich CIGS is largest at 406 K. The focus of this paper is not on the phase transition, and we did not determine the exact transition temperature. Figure 1(c) and 1(d) shows snapshots of a demixed state at 348 K and a mixed state at 406 K, respectively. Both simulations started with an ordered system of periodic unit cells [Fig. 1(b)].

It is interesting to compare our results to recent photoluminescence experiments by Gütay and Bauer, who measured the local band gaps on a CIGS surface. Scanning 40 000 pixels of 200 nm width, they found a Gaussian-like distribution of band gaps with a FWHM (full width of half maximum) of 8 meV [21]. The histograms of our data can be translated into band-gap distributions, by using the band gaps of the respective Ga concentrations [22]. If we increase the size of our segments (i.e., the number of atoms in it) by a factor of N, the relative width of the histograms decreases approximately as $1/\sqrt{N}$. Extrapolation shows that a segment width of 200 nm ($346 \times 346 \times 1$ unit cells) leads to a FWHM of 1 meV for 870 K and 2 meV for 406 K. In this temperature region, the band-gap fluctuations grow strongly with decreasing temperature. The experimental FWHM of 8 meV includes surface and volume defects that are not considered in the calculations. Nevertheless, the In-Ga disorder contributes significantly to band-gap fluctuations.

For further analysis we define clusters of In (Ga) as a number of joint In (Ga) atoms. A low number of clusters with a high average cluster size is a sign for high inhomogeneity. We look at clusters of the minority atom species: Ga in In-rich CIGS and In in Ga-rich CIGS. Figure 3 shows

TABLE I. Standard deviation σ for In-rich and Ga-rich CIGS and relative difference.

Temperature (K)	σ (In-rich)	σ (Ga-rich)	$\frac{\sigma(\text{Ga-rich})}{\sigma(\text{In-rich})} - 1$
290	4.97	5.16	3.8%
348	3.96	4.24	7.1%
406	2.39	2.61	9.2%
464	2.18	2.31	6.0%
522	2.07	2.19	5.8%
580	2.03	2.10	3.4%
638	1.99	2.06	3.5%
696	1.96	2.01	2.6%
754	1.93	1.97	2.1%
812	1.91	1.95	2.1%
870	1.90	1.93	1.6%

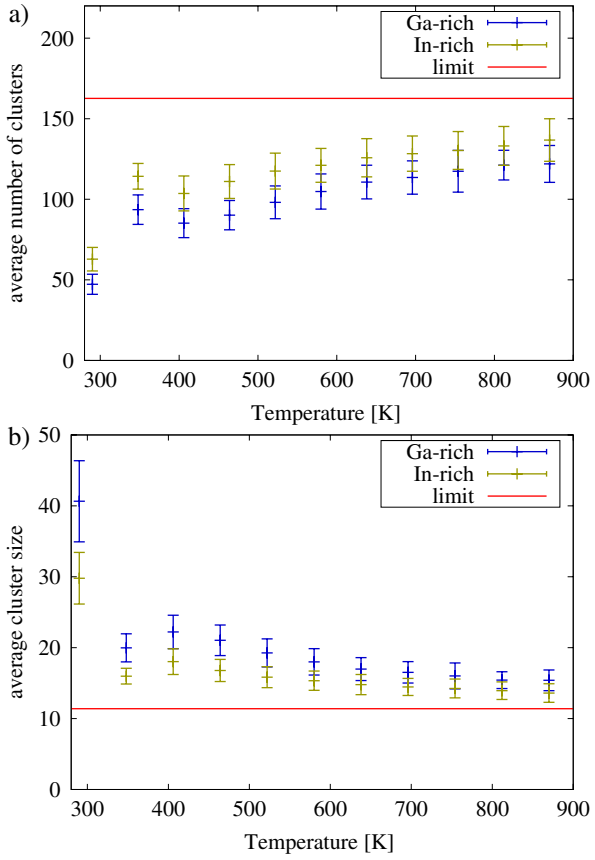

FIG. 3 (color online). Average number of clusters (a) and size of clusters (b) for Ga-rich and In-rich CIGS. Data points are the average value of all data sets of an MC run, and error bars are the standard deviation. The blue lines give the limit for simulations with infinite temperature. The considered clusters are connected In atoms in Ga-rich CIGS and connected Ga atoms in In-rich CIGS.

the average number of clusters and cluster size for In-rich and Ga-rich CIGS. Data were taken at several temperatures between 290 and 870 K. At all temperatures the number of clusters is higher and the size of clusters is lower for In-rich CIGS, confirming the fact that Ga-rich CIGS is more inhomogeneous. The data show a continuous increase of the average number of clusters with temperature for both systems, apart from a small peak at 348 K (near the phase transition). The increase is rapid below 348 K and slower above 406 K. The average size of clusters shows the opposite trend: rapid decrease below 348 K, a dip at 348 K, and a slower decrease above 406 K. The horizontal lines in both graphs mark the limits that were obtained in simulations with infinite temperature.

Calculations with larger simulation boxes ($24 \times 24 \times 12$) show that finite size effects do not play a role for these results. The size of the clusters is independent of the volume, as is the ratio number of (clusters):(volume).

Ab initio–based MC simulations of $CuIn_xGa_{1-x}Se_2$ revealed strong fluctuations in the spatial In-Ga distribution, caused by a demixing transition near room temperature. The In-Ga disorder plays an important role for band-gap fluctuations. We found that In-rich CIGS exhibits a higher homogeneity than Ga-rich CIGS at all considered temperatures between room temperature and the production temperature of solar cells. This is in agreement with experiments of Gütay and Bauer [6]. The effect of cluster size dependence on Ga content provides a possible explanation for the relatively low efficiency of CIGS with high Ga content (low as compared to what could be excepted from their band gap in the homogeneous case).

Our results show that inhomogeneities become strongly pronounced as the material is slowly cooled down to room temperature, undergoing the demixing transition. The lack of phase separation in actual solar cells shows that the In-Ga distribution is ''frozen'' in a high-temperature state. In order to minimize band-gap fluctuations, the frozen state must correspond to a rather high-temperature value. Thus, higher production temperatures and a reasonably fast cooling will lead to better efficiencies, which has recently been shown experimentally [23].

The authors thank Axel van de Walle for help with the ATAT [24,25] program package. This work was funded by the German Bundesministerium für Umwelt, Naturschutz und Reaktorsicherheit (Project No. 0327665A).

[1] M. Gloeckler, J. R. Sites, and W. K. Metzger, J. Appl. Phys. **98**, 113704 (2005).
[2] M. Hetzer, Y. Strzhemechny, M. Gao, M. Contreras, A. Zunger, and L. Brillson, Appl. Phys. Lett. **86**, 162105 (2005).
[3] S. Zhang, S.-H. Wei, A. Zunger, and H. Katayama-Yoshida, Phys. Rev. B **57**, 9642 (1998).
[4] C. Persson, Y.-J. Zhao, S. Lany, and A. Zunger, Phys. Rev. B **72**, 035211 (2005).
[5] D. Liao and A. Rockett, J. Appl. Phys. **91**, 1978 (2002).
[6] L. Gütay and G. Bauer, Thin Solid Films **515**, 6212 (2007).
[7] C.-H. Huang, J. Phys. Chem. Solids **69**, 330 (2008).
[8] S.-H. Wei, S. Zhang, and A. Zunger, Appl. Phys. Lett. **72**, 3199 (1998).
[9] M. Green, K. Emery, D. King, S. Igari, and W. Warta, Prog. Photovoltaics **13**, 49 (2005).
[10] J. Werner, J. Mattheis, and U. Rau, Thin Solid Films **480**, 399 (2005).
[11] L. Gütay and G. Bauer, Thin Solid Films **517**, 2222 (2009).
[12] Y. Yan, R. Noufi, K. Jones, K. Ramanathan, M. Al-Jassim, and B. Stanbery, Appl. Phys. Lett. **87**, 121904 (2005).
[13] N. Rega, S. Siebentritt, J. Albert, S. Nishiwaki, A. Zajogin, M. Lux-Steiner, R. Kniese, and M. Romero, Thin Solid Films **480**, 286 (2005).
[14] J. Jaffe and A. Zunger, Phys. Rev. B **28**, 5822 (1983).
[15] J. Sanchez, F. Ducastelle, and D. Gratias, Physica (Amsterdam) **128A**, 334 (1984).
[16] S. Müller, J. Phys. Condens. Matter **15**, R1429 (2003).
[17] The ABINIT code is a common project of the Université Catholique de Louvain, Corning Inc., and other contributors (http://www.abinit.org).
[18] X. Gonze *et al.*, Comput. Mater. Sci. **25**, 478 (2002).
[19] J. P. Perdew, K. Burke, and M. Ernzerhof, Phys. Rev. Lett. **77**, 3865 (1996).
[20] D. B. Laks, L. Ferreira, S. Froyen, and A. Zunger, Phys. Rev. B **46**, 12 587 (1992).
[21] L. Gütay and G. Bauer, in *Proceedings of the 34th IEEE Photovoltaic Specialists Conference* (IEEE, New York, 2009).
[22] S.-H. Wei and A. Zunger, J. Appl. Phys. **78**, 3846 (1995).
[23] J. Windeln *et al.*, in *Proceedings of the 24th European Photovoltaic Solar Energy Conference* (World Scientific, Munich, 2009), p. 2443.
[24] A. van de Walle and G. Ceder, J. Phase Equilib. **23**, 348 (2002).
[25] A. van de Walle, M. Asta, and G. Ceder, CALPHAD: Comput. Coupling Phase Diagrams Thermochem. **26**, 539 (2002).